Bioorg. Med. Chem. Lett. 41 (2021) 127923

Contents lists available at ScienceDirect

Bioorganic & Medicinal Chemistry Letters

journal homepage: www.elsevier.com/locate/bmcl

Novel pyrazolo[4,3-*d*]pyrimidine microtubule targeting agents (MTAs): Synthesis, structure–activity relationship, *in vitro* and *in vivo* evaluation as antitumor agents

Farhana Islam [a], Tasdique M. Quadery [a], Ruoli Bai [b], Lerin R. Luckett-Chastain [c], Ernest Hamel [b], Michael A. Ihnat [c], Aleem Gangjee [a,*]

[a] Division of Medicinal Chemistry, Graduate School of Pharmaceutical Sciences, Duquesne University, 600 Forbes Avenue, Pittsburgh, PA 15282, United States
[b] Molecular Pharmacology Branch, Developmental Therapeutics Program, Division of Cancer Treatment and Diagnosis, Frederick National Laboratory for Cancer Research, National Cancer Institute, National Institutes of Health, Frederick, MD 21702, United States
[c] Department of Pharmaceutical Sciences, The University of Oklahoma College of Pharmacy, Oklahoma City, OK 73117, United States

ARTICLE INFO

Keywords:
Microtubule targeting agents
Structure–activity relationship
Pyrazolo[4,3-*d*]pyrimidine
Colchicine site
Nuclear Overhauser Effect spectroscopy

ABSTRACT

The design, synthesis, and biological evaluation of a series novel *N*1-methyl pyrazolo[4,3-*d*]pyrimidines as inhibitors of tubulin polymerization and colchicine binding were described here. Synthesis of target compounds involved alkylation of the pyrazolo scaffold, which afforded two regioisomers. These were separated, characterized and identified with ^{1}H NMR and NOESY spectroscopy. All compounds, except **10**, inhibited [^{3}H] colchicine binding to tubulin, and the potent inhibition was similar to that obtained with CA-4. Compounds **9** and **11**–**13** strongly inhibited the polymerization of tubulin, with IC_{50} values of 0.45, 0.42, 0.49 and 0.42 μM, respectively. Compounds **14**–**16** inhibited the polymerization of tubulin with IC_{50s} near ~1 μM. Compounds **9**, **12**, **13** and **16** inhibited MCF-7 breast cancer cell lines and circumvented βIII-tubulin mediated cancer cell resistance to taxanes and other MTAs, and compounds **9**–**17** circumvented Pgp-mediated drug resistance. In the standard NCI testing protocol, compound **9** exhibited excellent potency with low to sub nanomolar GI_{50} values (≤10 nM) against most tumor cell lines, including several multidrug resistant phenotypes. Compound **9** was significantly ($P < 0.0001$) better than paclitaxel at reducing MCF-7 TUBB3 (βIII-tubulin overexpressing) tumors in a mouse xenograft model. Collectively, these studies support the further preclinical development of the pyrazolo[4,3-*d*]pyrimidine scaffold as a new generation of tubulin inhibitors and **9** as an anticancer agent with advantages over paclitaxel.

Cancer is the second-largest cause of mortality in the world and accounted for an estimated 9.6 million deaths in 2018.[1] An effective strategy for cancer therapy is to target the mitotic pathways of rapidly proliferating tumor cells.[2] Microtubules are hollow tube-like assemblies consisting of heterodimers of two globular protein subunits, α- and β-tubulin (Fig. 1). Tubulin dimers are longitudinally arrayed to form protofilaments, and the protofilaments in turn interact laterally to form the microtubule[3] (Fig. 1). Microtubules play essential roles in multiple eukaryotic cellular processes, such as cell growth and division, motility, intracellular trafficking, and the ability to adapt cellular shape in response to the environment.[4] Molecules that bind to tubulin and interrupt the dynamics of microtubules can be classified as microtubule targeting agents (MTAs),[4] which possess highly diverse chemical structures, a few of which are shown in Figure 2.[5,6]

Chemotherapy with MTAs has led to improvement in the duration and quality of life for many patients with cancer.[7] Despite their success, there are several shortcomings associated with MTAs. Treatment with MTAs can result in drug resistance that often is a major obstacle to treatment success.[7] The clinical utility of the taxanes and the vinca alkaloids is severely limited by two major mechanisms of drug resistance:

Abbreviations: CS, colchicine site; CA-1, combretastatin A-1; CA-4, combretastatin A-4; CA-4P, combretastatin A-4 phosphate; DMSO, dimethyl sulfoxide; DIPEA, *N,N*-Diisopropylethylamine; (MTAs, microtubule targeting agents; NCI, National Cancer Institute; NOESY, Nuclear Overhauser Effect Spectroscopy; Pgp, P-glycoprotein; (PDB, Protein Data Bank; SRB, sulforhodamine B; TFA, trifluoracetic acid.

* Corresponding author at: Division of Medicinal Chemistry, Graduate School of Pharmaceutical Sciences, Duquesne University, 600 Forbes Avenue, Pittsburgh, PA 15282, United States.

E-mail address: gangjee@duq.edu (A. Gangjee).

https://doi.org/10.1016/j.bmcl.2021.127923
Received 4 December 2020; Received in revised form 25 February 2021; Accepted 25 February 2021
Available online 9 March 2021

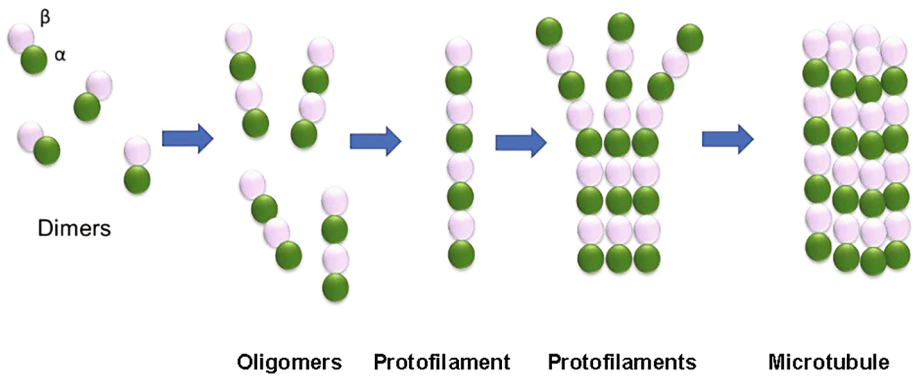

Fig. 1. Formation of microtubules: polymerization of dimers of α- and β-tubulin, formation of protofilaments and finally cyclization into microtubules. (Modified from Kaul et al.[26]).

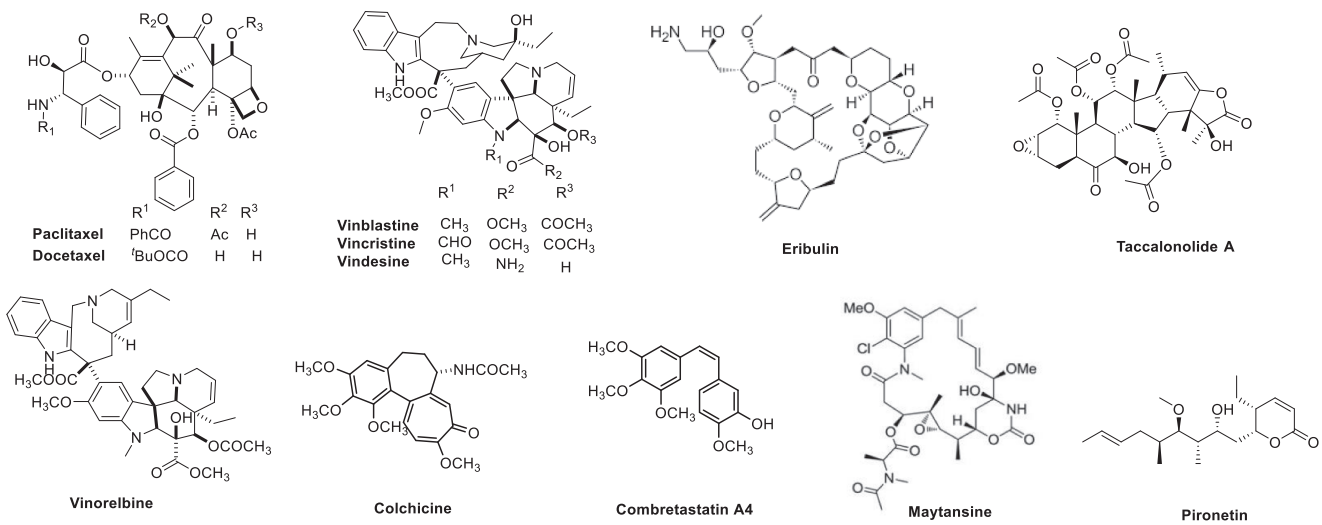

Fig. 2. Representative microtubule targeting agents.

the expression of the drug efflux pump P-glycoprotein (Pgp) and overexpression of the βIII-isotype of tubulin.[8,9] Pgp expression is very common, particularly in patients who have received prior chemotherapy.[10] The use of Pgp inhibitors to overcome this resistance has been explored but is unsuccessful due to side effects, which occur with high doses.[11] The overexpression of βIII-tubulin is involved in clinical resistance to taxanes and vinca alkaloids in nonsmall cell lung,[12,13] breast,[14] ovarian,[15] and gastric[16] cancers. In addition to the resistance issues, the complex natural product MTAs have neurotoxicity, low oral bioavailability and narrow therapeutic indexes as major impediments to clinical success.[17–19]

Many reports have shown that CS agents frequently do not display either Pgp or βIII-isotype dependent resistance.[20] Thus, development of MTAs targeting the CS can circumvent the resistance limitations associated with taxanes and vinca alkaloids, and their use should improve clinical outcomes.[21,22] Colchicine itself is an approved drug for gout but is not employed as an anticancer agent due to its toxic side effects at higher doses. These include neutropenia, gastrointestinal upset, bone marrow damage, and anemia.[23] Other colchicine binding inhibitors have demonstrated promise and some are currently in clinical trials as

Table 1
Microtubule depolymerization activity, antiproliferative effects, inhibition of colchicine binding and tubulin assembly.

The increase of activity of lead compounds with a 5-methyl group					
No	Cellular microtubule depolymerization EC_{50} (nM)	Antiproliferative effects MDA-MB-435 IC_{50} (nM) ± SD	Inhibition of colchicine binding		Inhibition of tubulin assembly IC_{50} (μM ± SD)
			5 μM inhibitor % inhibition ± SD	0.5 μM inhibitor% inhibition ± SD	
1	>10000	ND	0	ND	ND
2	1200	96 ± 5	60 ± 1	ND	10 ± 0.6
3	7.4	4.3 ± 0.3	99 ± 2	79 ± 0.8	ND
4	–	–	ND	ND	21 ± 1
5	–	–	92 ± 0.2	73 ± 3	0.48 ± 0.008
6	–	–	43 ± 3	ND	3.3 ± 0.3
7	–	–	72 ± 2	ND	0.91 ± 0.03
CA-4	9.8	4.4 ± 0.5	99 ± 0.8	84 ± 3	0.54 ± 0.06

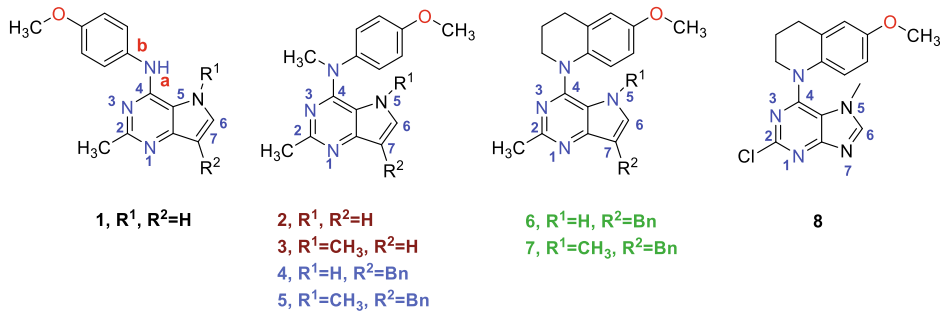

Fig. 3. Lead compounds.

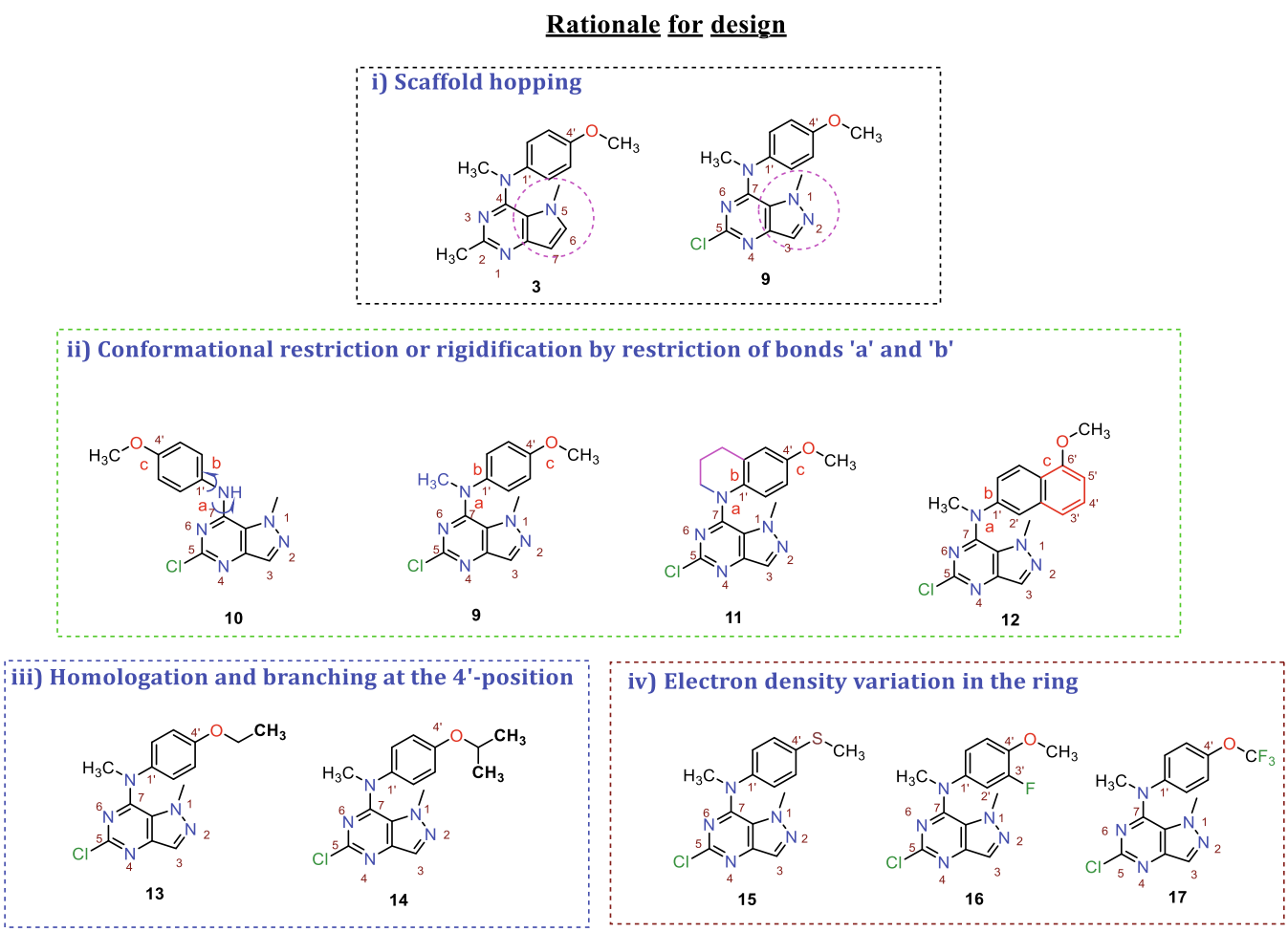

Fig. 4. Compounds 9–17 and the rationale for drug design.

anticancer candidates.[24]

One of the most potent anti-mitotic CS MTAs that gained the attention of medicinal chemists and cancer biologists is combretastatin A-4 (CA-4, Fig. 2), a trimethoxyphenyl (TMP) containing stilbenoid.[21] CS inhibitors have been extensively studied, and several have entered clinical trials, including 2-methoxyestradiol, combretastatin A-4 phosphate (CA-4P) (fosbretabulin), the combretastain CA-1P prodrug OXi4503 (3-methoxy-2-phosphonooxy-6-[(*Z*)-2-(3,4,5-trimethoxyphenyl)ethenyl]phenyl] dihydrogen phosphate), AVE8062 ((2*S*)-2-Amino-3-hydroxy-*N*-[2-methoxy-5-[(*Z*)-2-(3,4,5-trimethoxyphenyl)ethenyl]phenyl]propenamide), CKD-516 ((*S*)-*N*-(4-(3-(1*H*-1,2,4-triazol-1-yl)-4-(3,4,5-trimethoxybenzoyl)phenyl)thiazol-2-yl)-2-amino-3-methylbutanamide hydrochloride), BNC105P (sodium 6-methoxy-2-methyl-3-(3,4,5-trimethoxybenzoyl)benzofuran-7-yl phosphate), ABT-751 (*N*-[2-(4-hydroxyanilino)pyridin-3-yl]-4-methoxybenzenesulfonamide), CYT-997 (1-ethyl-3-[2-methoxy-4-[5-methyl-4-[[(1*S*)-1-pyridin-3-ylbutyl]amino] pyrimidin-2-yl]phenyl]urea), ZD6126 (phosphoric acid mono-(5-acetylamino-9,10,11-trimethoxy-6,7-dihydro-5*H*-dibenzo[*a*,*c*]cyclohepten-3-yl) ester), plinabulin (NPI-2358); ((3*Z*,6*Z*)-3-benzylidene-6-[(5-*tert*-butyl-1*H*-imidazol-4-yl)methylidene]piperazine-2,5-dione), MN-029 (methyl *N*-[6-[4-[[(2*S*)-2-aminopropanoyl]amino]phenyl]sulfanyl-1*H*-benzimidazol-2-yl]carbamate).[13,14,25] Currently there are no CS agents approved by the FDA for cancer, and this demonstrates the need to develop additional CS agents for potential clinical use[7] because

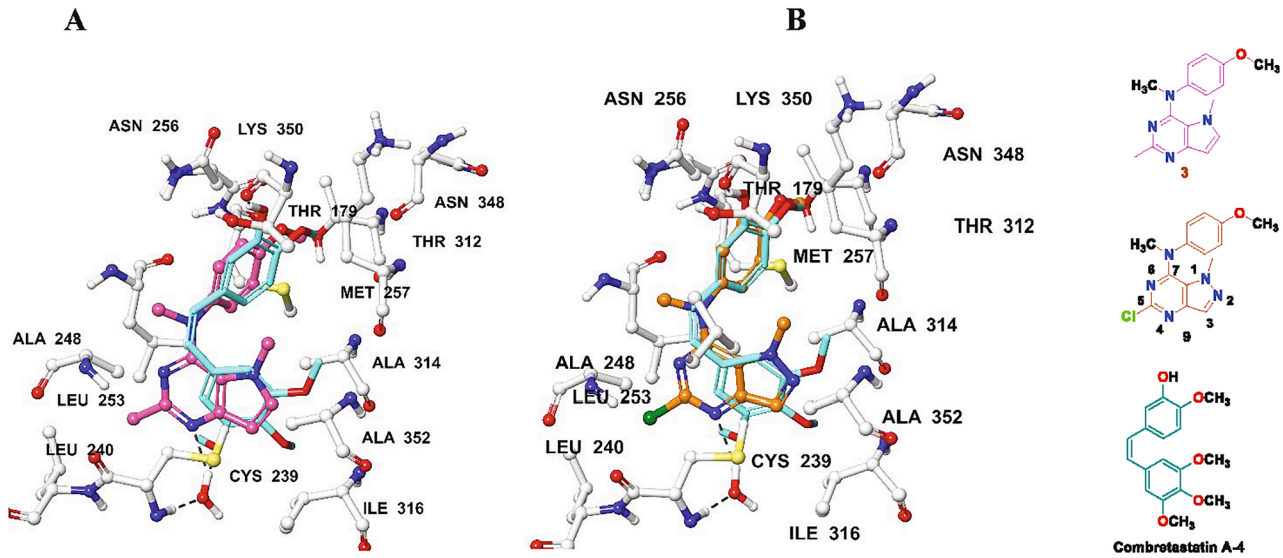

Fig. 5. A) Docked pose of lead 3 (pink) with CA-4 (cyan) in the CS. B) Docked pose of 9 (tan) with CA-4 (cyan) in the CS. (Maestro 2020-2. Docked scores of 3 and 9 are −9.76 and −10.71 kcal/mol, respectively).

overcoming Pgp and βIII-tubulin mediated resistance is required to improve the overall survival rates observed with MTAs currently in clinical use.

We previously reported[27,28] compounds **2**–**7** (Table 1 and Fig. 3) as potent CS antiproliferative agents. In the structure–activity relationship (SAR) studies of these pyrrolo[3,2-*d*]pyrimidine based antitubulin agents, we demonstrated the importance of the 5-methyl moiety on compounds **3, 5** and **7** for significant improvement of biological activities over the 5-desmethyl compounds **2, 4** and **6**. Compound **3** with a 5-methyl is 160- and 22-fold more potent in cellular microtubule depolymerization activity and antiproliferative effects, respectively than the corresponding 5-desmethyl **2**. Moreover, compounds **5** and **7** are 43- and 4-fold more potent in inhibiting tubulin assembly respectively, than compounds **4** and **6**. On the basis of our previous studies it was of interest to design a novel series of *N*1-methylated pyrazolo[4,3-*d*]pyrimidines (Fig. 4) as potential MTAs and as anticancer agents. As the first step of our efforts, we utilized scaffold hopping on the pyrrolo[3,2-*d*] pyrimidines as an approach to design novel pyrazolo[4,3-*d*]pyrimidines. Scaffold hopping is a drug design strategy to identify structurally diverse compounds that are similar in activity/property space.[29] An additional aspect incorporated into the pyrazolo[4,3-*d*]pyrimidine structure was a 2-chloro substituent. It was observed that a 2-chloro substituted purine compound **8** displayed IC_{50} values of 39.6 ± 2.9, 41.2 ± 3.2 and 58.9 ± 3.1 nM in three human malignant melanoma cell lines A375, M14 and RPMI7951, respectively.[30] Thus, it was of interest to explore the antitumor activity of these compounds with the novel *N*1-methyl-pyrazolo[4,3-*d*]pyrimidine scaffold with a chlorine substitution at the 5-position as MTAs. We used various additional structural modifications for the design of compounds **9**–**17** (Fig. 4) that include d i) rigidification or conformational restrictions, ii) homologation and branching on the alkyl chain and iii) variation in electronic effects on the aromatic ring.

Our optimization effort started by replacing the pyrrole ring in **3**

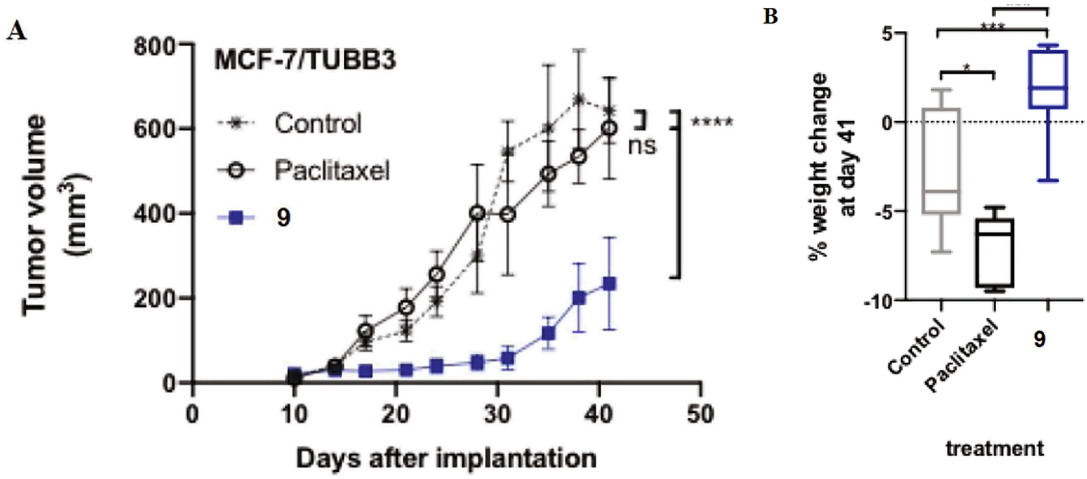

Fig. 6. Treatment with compound 9 decreased primary tumor growth in MCF-7 TUBB3 (βIII-tubulin overexpressing) breast cancer cell model. * = P < 0.05; *** P < 0.001 (0.0007 for control vs 9, 0.0003 for PTX vs 9. A) 10^7 cells/100 uL Matrigel as implanted into fat pad #4 of 8 wk old athymic female mice. The mice were treated with compound 9 at the maximally tolerated dose (MTD) of 30 mg/kg two times weekly or with paclitaxel at its MTD of 10 mg/kg/week and tumor volumes were determined. Statistical analysis was performed with two-way ANOVA repeated measures post test. Compound 9 was significantly (P < 0.0001) better than paclitaxel at reducing MCF-7 TUBB3 (βIII-tubulin overexpressing) tumor volume. B) Animal weights were graphed as percent weight change at day 41 over the starting weight. Statistical analysis was performed with one-way ANOVA. Only the control and paclitaxel mice lost weight at the end of the study. Sample sizes are 7 for control (an animal was lost toward the end of the experiment) and 8 for PTX and 9.

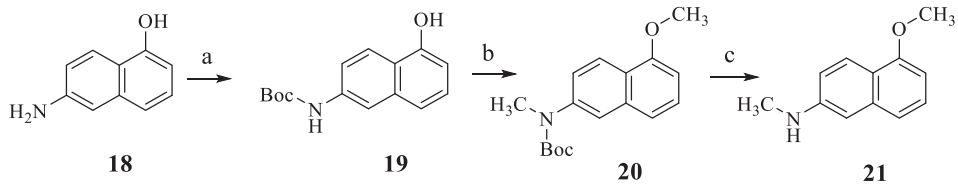

Scheme 1. a) Di-*tert*-butyl dicarbonate, DCM, rt, 4 h, 72%; b) CH_3I, DMF, rt, 12 h, 55%; c) CF_3COOH, THF, rt, 6 h, 69%.

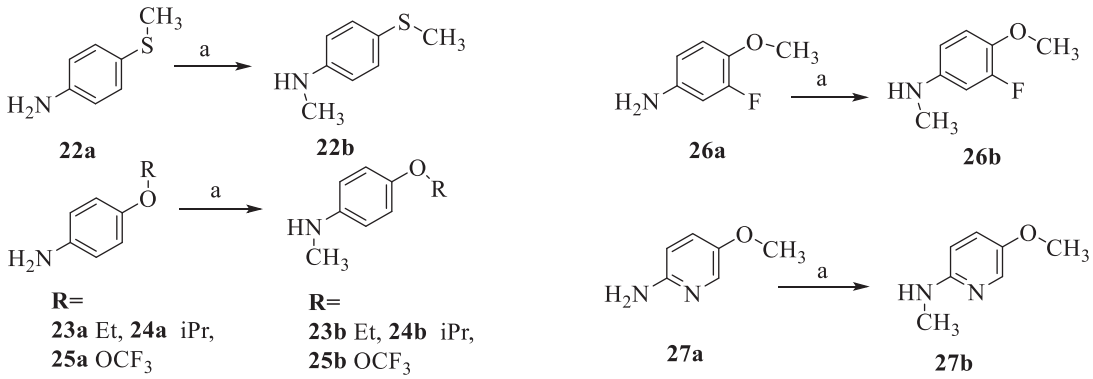

Scheme 2. i) Paraformaldehyde, DCM, 12 h; ii) $NaBH_4$, DCM, rt, 6-12 h, 56-72% over two steps.

with a pyrazolo ring and a 5-chloro group to afford compound **9**. Using molecular modeling (Maestro 2020–2),[31] we docked several conformationally restricted analogs in the CS of tubulin. As shown in Fig. 4, the bioactive conformations of **9** and **10** are determined by three rotatable single bonds: 4-position C—N bond (bond *a*), 1′-position C—N bond (bond *b*) and 4′-position C—O bond (bond *c*). Literature findings[32] suggest that conformational preference via molecular modeling and ^{1}H NMR studies indicate that a methyl group on the aniline nitrogen in **1** and **2** restricts the free rotation of both bond *a* and bond *b* (Fig. 3) and thus restricts the conformation of the anilino ring. Conformational constraint of a small-molecule inhibitor can enhance the binding affinity to its intended target protein by reducing conformational entropic costs upon binding and can also improve the binding selectivity by reducing accessible, low-energy conformational space.[33,34] We, therefore, modeled the conformationally restricted analogs **9**, **11**, and **12**. In compound **9**, the restriction of bond *a* was accomplished by incorporating a *N*7-methyl group in **10**. Compound **11**, with the 1,2,3,4-tetrahydroquinoline at the *N*7-position was designed from **9** by further restricting bond *b*. Compound **12** restricts both bonds *a* and *b* by incorporating a fused bicyclic 6′-methoxynaphthyl-1′-amino ring at the *N*7-position as a replacement of the monocyclic 4′-methoxyphenyl group of **9**. In compounds **9**, **11** and **12**, bond rotation restrictions were anticipated to reduce the energy to adopt the bound conformation, thus allowing improved inhibitory activity.

Next, we focused on the homologation and branching of the 4′-OMe (**9**) to 4′-OEt (**13**) and 4′-O-iPr (**14**) to allow for better penetration into the hydrophobic pocket of the CS. We also explored the impact of electron density and hydrogen bonding ability in compounds **15**–**17**. The distance and the nature of heteroatom substitution affects hydrogen bond (HB) strength.[35] Thus, it was of interest to isosterically replace the oxygen atom of the 4′-OCH_3 of **9** with a sulfur and synthesize **15**. Compounds **16** and **17** were designed and synthesized to probe the electron withdrawing effect of fluorine on the inhibition of colchicine binding and microtubule assembly and on anticancer activity.

Compounds **1**–**17** were docked in the X-ray crystal structure of the CS (PDB: 6BS2, 2.65 Å)[30] using Maestro, Schrödinger 2020–2.[31] Multiple low energy conformations were obtained from docking. Fig. 5 shows the docked conformation of lead **3** (pink) and compound **9** (tan) superposed with CA-4 (cyan). The pyrazolo[4,3-*d*]pyrimidine scaffold of **9**–**17** form hydrophobic interactions at the *αβ* tubulin interface with Alaβ314,

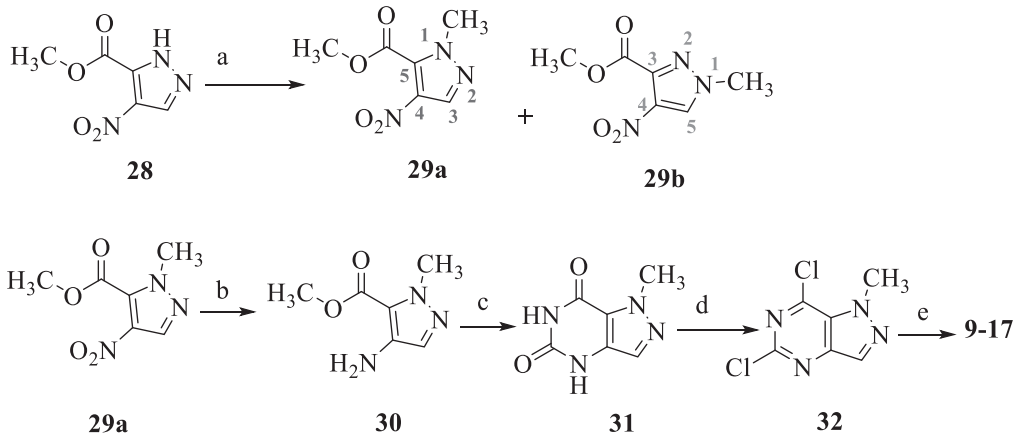

Scheme 3. CH_3I, K_2CO_3, DMF, rt, 12 h (29a: 35%, 29b: 55%) ; b) 10% Pd/C, H_2, MeOH, 40 psi, 1 h, 72%; c) urea, 180 °C, 2 h; d) $POCl_3$, pyridine, toluene, 4 h, reflux, 42%; e) anilines, acetonitrile, reflux, 4–12 h, 35–49%.

Table 2
Inhibition of colchicine binding and tubulin assembly.

Compound No	Inhibition of colchicine binding		Inhibition of tubulin assembly IC_{50} (μM ± SD)
	5 μM inhibitor % inhibition ± SD	0.5 μM inhibitor% inhibition ± SD	
2	60 ± 1	ND	10 ± 0.6
3	99 ± 2	79 ± 0.8	ND
4	ND	ND	21 ± 1
5	92 ± 0.2	73 ± 3	0.48 ± 0.008
6	43 ± 3	ND	3.3 ± 0.3
7	72 ± 2.0	ND	0.91 ± 0.03
9	94 ± 3	68 ± 3	0.45 ± 0.09
10	7.1 ± 3	–	>20
11	94 ± 0.4	68 ± 2	0.42 ± 0.07
12	91 ± 1	66 ± 0.7	0.49 ± 0.01
13	99 ± 0.4	88 ± 0.007	0.42 ± 0.07
14	85 ± 1	–	1.1 ± 0.08
15	93 ± 0.5	64 ± 2	0.82 ± 0.02
16	97 ± 0.3	77 ± 1	0.74 ± 0.04
17	64 ± 5	–	2.9 ± 0.2
CA-4	99 ± 0.8	84 ± 3	0.54 ± 0.06

Alaβ352 and Ileuβ316 similar to the lead pyrrolo[3,2-*d*]pyrimidine scaffold. The pyrazole ring is stacked amid the Metβ257 and Cysβ239. The *N7*-CH_3 moiety of **9** and **11**–**17** forms hydrophobic interactions with Alaβ314 and Leuβ253. The 4′-oxygen of compounds **9**–**14**, and **16**–**17** and the 4′-sulfur of compound **15** are oriented towards the pocket formed by Thrα179, Lysβ350, Asnβ256 and Asnβ348. The 5-Cl of **9**–**17** makes hydrophobic interactions with Leuβ253 and Leuβ240 (only **9** is shown in Fig. 5B). The *N4* of the pyrazolo[4,3-*d*]pyrimidine ring of all the compounds makes water mediated hydrogen bond interactions with the backbone of Cysβ239 similar to the original X-ray crystallized ligand.[30] The docked score of compound **9** is −10.71 kcal/mol and is better than the lead compound **3** (−9.76 kcal/mol). The docked scores for **10** is −9.32, and for **11**–**17** are in a range of −9.95 to −10.65 kcal/mol. The *N7*-desmethyl compound **10** has the lowest docked score of the designed analogs and was predicted to be the least active.Fig. 6

Boc-protection of **18** afforded **19** in 72% yield. Methylation of **19** to **20** and subsequent deprotection[36] provided the aniline intermediate **21** (Scheme 1). Treatment of **22a-27a** with paraformaldehyde, followed by reduction with $NaBH_4$ gave the anilino intermediates **22b-27b** (Scheme 2). In Scheme 3, pyrazole **28** was alkylated with methyl iodide in the presence of base K_2CO_3 in DMF, to provide after separation two regioisomers, **29a** and **29b**, in 35 and 55% yields, respectively. Intermediates **29a** and **29b** were characterized by ^{1}H NMR and NOESY (Nuclear Overhauser Enhancement Exchange Spectroscopy). Varying the base has been used in the literature to alkylate the N1 position.[37,38] Our use of K_2CO_3 is the first reported to yield **29a** and **29b** in 35 and 55% yields, respectively. The separation method is discussed in the Experimental Section. The ^{1}H NMRs of **29a** and **29b** agree with those in the literature.[39] Reduction of the nitro group in **29a**, yielded **30**, which was cyclized to **31** with urea. Chlorination of **31** with $POCl_3$ and pyridine in toluene provided **32**. Nucleophilic aromatic substitution of **32** using anilines 4′-methoxyaniline, 4′-methoxy-*N*-methylaniline, **21**, **22b-27b** afforded final compounds **9**–**17** in 68–84% yields.

Compounds **9**–**17** and the reference compound CA-4 were evaluated for inhibitory effects on tubulin polymerization and on the binding of [^{3}H]colchicine to tubulin as an indication of whether their antiproliferative effects are the result of an interaction with tubulin (Table 2). CA-4 is a drug candidate in clinical trials,[40,41] and it is a highly potent, competitive inhibitor of the binding of colchicine to tubulin.[42] Except for **10**, all the compounds at, 5 μM, inhibited [^{3}H]colchicine binding to the protein, and the extent of inhibition was similar to that obtained with CA-4. With equal or more than 94% and 68% inhibition at 5 and 0.5 μM, respectively, compounds **9**, **11**, **13** and **16** showed similar potency as the lead compounds and CA-4 (Tables 1 and 2). Isosteric replacement of 4′-OMe with 4′-SMe generated compound **15**, which was equipotent to **9** in the inhibition of colchicine binding assay. Compounds **11** and **12**, the conformationally restricted analogs of **9**, in the colchicine binding assay (Table 2), displayed comparable potency to **9** (94 and 91% at 5 μM and 68 and 66% at 0.5 μM, respectively). Next, we assessed the effects of homologation and branching at the 4′-O-position of **9**. Homologation with a single methylene at the 4′-position of **9** (4′-OMe) afforded **13** (4′-OEt), which was more potent (99% at 5 μM and 88% at 0.5 μM) than both **9** and CA-4 in the colchicine inhibition assay. Branching with an isopropyl moiety afforded compound **14**, which was slightly less potent than **9**, with 85% inhibition at 5 μM. Introduction of a fluorine atom at the 3′-position of the phenyl ring of **9** yielded compound **16**, which had 97 and 77% inhibition at 5 and 0.5 μM, respectively, in the inhibition of colchicine binding assay. Compounds **11**–**16** at 5 μM, inhibited the binding of [^{3}H]colchicine by 85–99%, whereas compound **17** showed only a 64% inhibition at 5 μM of [^{3}H]colchicine binding. Compound **10** was completely inactive in inhibiting colchicine binding. The lower activity of **17** could be attributed to the strong electron withdrawing effect of the CF_3 moiety on the oxygen of the 4′-position. This oxygen (or sulfur in **16**) does interact with the pocket formed by Thrα179, Lysβ350, Asnβ256 and Asnβ348 at the colchicine site, and the CF_3 reduces this interaction. Compound **10**, lacking the *N7*-methyl moiety, did not inhibit tubulin assembly, nor did it have a significant effect on colchicine binding, emphasizing the critical role of this methyl moiety at the *N7*-position in retaining the bioactive conformation for anti-tubulin activity (described below). The lack of activity of **10** corroborates the lowest docked score of **10** in the CS obtained from our molecular modeling studies.

Table 3
Activities of compounds 9, 12, 13 and 16 in a *βIII*-tubulin overexpressing cell line.

Agent	MCF-7 WT EC_{50} (nM)	MCF-7 TUBB3 *βIII*-tubulin EC_{50} (nM)	Resistance Ratio MCF-7 TUBB3/WT
9	2.0 ± 0.3	3.3 ± 0.4	1.1
12	35.2 ± 4.7	16.8 ± 1.5	0.5
13	7.7 ± 0.7	9.7 ± 1.0	1.3
16	1.7 ± 0.2	2.6 ± 0.4	1.6
Paclitaxel	194.2	2065.8	10.6

All of the compounds (except **10**) were highly active in the tubulin assembly assay with low to sub micromolar inhibitory IC_{50} values (0.42–1.1 μM), comparable with lead compounds **5** and **7** (0.48 and 0.91 μM, respectively) and CA-4 (0.54 μM) (Table 2). Compounds **9** and **11**–**13** strongly inhibited the polymerization of tubulin, with IC_{50} values 0.45, 0.42, 0.49 and 0.42 μM, respectively. Compound **10** had no effect on tubulin polymerization. Compounds **14**–**16** inhibited the polymerization of tubulin with an IC_{50s} near ~1 μM, 2-fold less potent than CA-4.

The potent MTAs **9**, **12**, **13** and **16** were selected for evaluation of their inhibitory activities towards the growth of MCF-7 wild-type (WT) human breast cancer cells and and a MCF-7 cell line overexpressing *βIII*-tubulin (data shown in Table 3). Comparing the EC_{50} values in these cell lines, compounds **9** and **16** were the most potent of the series (EC_{50}s 2.0 and 3.3 nM for **9** and 1.7 and 2.6 nM for **16** in MCF-7 WT and MCF7-*βIII*-tubulin overexpressing cell lines, respectively). Compounds **9** and **16** were 100- and ~600-fold, respectively more active than paclitaxel in the MCF-7 WT and MCF-7-*βIII*-tubulin cell lines. On the other hand, compounds **12** and **13** were 5- and 25-fold more potent, respectively, in the MCF-7 WT cells; and 120- and 220-fold more potent, respectively, in the MCF-7-*βIII*-tubulin cell line compared to paclitaxel. Comparison of the EC_{50} values in the parental MCF-7 WT and genetically manipulated MCF-7 *βIII* cell line allows for the calculation of a relative resistance value, designated as Rr. This value is calculated by dividing the EC_{50} value obtained in the *βIII*-overexpressing MCF-7 cells by the EC_{50} obtained in the parental MCF-7 WT cells. The isoform *βIII* is an important determinant in cellular resistance towards paclitaxel, which is a known

Table 4
Compound activity in a Pgp overexpressing cell line.

Compound No	Compound activity in a Pgp overexpressing cell line[a]		Rr
	Parental OVCAR-8 IC_{50} (nM) ± SD	Pgp overexpressing NCI/ADR-RES IC_{50} (nM) ± SD	
9	9.0 ± 0.7	5.0 ± 0	0.55
10	>5000	>5000	–
11	17 ± 2	8.0 ± 0.7	0.47
12	14 ± 3	11 ± 0.7	0.78
13	2.0 ± 1	4.0 ± 1	2.0
14	49.0 ± 10	44 ± 8.0	0.89
15	31 ± 2	17 ± 3	0.54
16	9.0 ± 1	7.0 ± 3	0.77
17	880 ± 40	730 ± 100	0.83
Paclitaxel	5.3 ± 2	800 ± 200	150
CA-4	1.8 ± 0.4	1.8 ± 0.4	1.0

Pgp substrate.[11,16] The Rr value of paclitaxel was 10.6 (resistance ratio: *βIII*-tubulin/WT). Compound **12** had an Rr of 0.5, indicating that it is able to overcome drug resistance mediated by *βIII*. Compounds **9**, **13**, and **16** also had Rr values ≤1.6, suggesting that they are all poor substrates for *βIII*-tubulin.

The ability of **9**–**17** to circumvent Pgp-mediated drug resistance was evaluated using an ovarian cancer cell line pair (Table 4). The Rr value is calculated by dividing the IC_{50} value obtained in the Pgp overexpressing NCI/ADR-RES cells by the IC_{50} obtained in the parental OVCAR-8 cells. The Rr value for paclitaxel was 150 whereas most of the synthesized compounds had Rr values less than 1. The <1 Rr values indicated that these compounds were poor substrates for Pgp and hence have minimal Pgp-mediated transport and consequently should have advantages over MTAs that are good Pgp substrates.

To determine its antitumor spectrum, compound **9** was tested in the National Cancer Institute's panel of 60 human tumor cell lines (NCI-60). As shown in Table 5, compound **9** exhibited excellent potency with low GI_{50} values ≤10 nM against most tumor cell lines, including many multidrug resistant phenotypes, in the standard NCI testing protocol. The GI_{50} values of **9** was single digit nanomolar in 19 tumor cell lines.

Compound **9** was selected for a tubulin III overexpressing, anti-microtubule drug resistant *in vivo* xenograft mouse study on the basis of its nanomolar potency *in vitro* in the NCI cancer cell line panel and its potent activities in inhibiting microtubule polymerization and colchicine binding assay. Compound **9** significantly reduced primary tumor growth vs paclitaxel in the tubulin III overexpressing MCF-7 TUBB3 orthotopic xenograft, with no significant weight loss in the study as opposed to paclitaxel, which resulted in significant weight loss. Thus compound **9** is effective *in vivo* against antimicrotubule drug resistant breast cancer.

N-Alkylation of the pyrazole scaffold **28** afforded two regioisomers, **29a** and **29b**. Methylation of unsymmetrically substituted pyrazole derivatives usually affords mixtures of both possible alkylated products.[39] The regiochemistry of both alkylated intermediates **29a** and **29b** was identified by ^{1}H NMR[39] and NOESY spectroscopy (Figs. 7 and 8). In ^{1}H NMR (only δ values are included, spectra not shown). For the *N1*-CH_3 protons the chemical shift for **29a** and **29b** occurred as singlets at 4.02 and 3.95 ppm, respectively. It is noteworthy that the presence of the adjacent C5-carboxylate to the *N1*-CH_3 in **29a** caused the *N1*-CH_3 protons of **29a** to shift ~0.1 ppm deshielded compared to the *N1*-CH_3 of **29b**. The initial studies involved NMR utilizing NOESY spectroscopy, which is one of the most direct ways to determine spatial proton-proton/proton-heteronucleus/heteronucleus-heteronucleus correlations within a molecule in the range up to 5 Å or less.[39,43] This is also an excellent method to determine solution conformation. Intermediate **29a** was identified as the methyl 1-methyl-4-nitro-1*H*-pyrazole-5-carboxylate regioisomer, as no strong NOE correlation was observed between the H3 proton and the *N1*-CH_3 protons (Fig. 7). Intermediate **29b** was determined to be the methyl 1-methyl-4-nitro-1*H*-pyrazole-3-carboxylate regioisomer, as a characteristic NOE correlation was observed between the H5 proton and the *N*1-CH_3 protons (Fig. 8). The observed H5 proton and *N1*-CH_3 cross peak (δ 8.95, 3.95) was dominated by scalar coupling effects, with evidence of only a NOE proton contributing to it in **29b**. For **29a**, the H3 proton occurs at δ 8.36, and, for **29b**, the H5 proton is at δ 8.95. The probable deshielding effects of the H5 proton in **29b** is due to the direct electron withdrawing effect of C-5. ^{1}H NMR and crystal structure from a previous report, along with the 2D NMR from our studies, confirm the structure of regioisomers **29a** and **29b** as designated.

The ^{1}H NMR spectra of the *N7*-H analog **10** (Fig. 9) and the *N7*-CH_3 analog **9** (Fig. 10) in DMSO-d6 afforded additional information related to conformational restriction in **9** as compared to **10**. For compound **9**, the "*N1*-CH_3" protons appeared at δ 3.04, whereas for **10** they were significantly deshielded at δ 4.35 ppm. This shielding of the "*N1*-CH_3" protons in **9** was attributed to a diamagnetic anisotropic effect in **9** arising from the proximity of the phenyl ring as shown in Fig. 11 (more favored *anti*-conformation for **9** on the basis of the *N7*-CH_3 and the *N1*-CH_3 groups). The steric bulk of the *N7*-CH_3 resulting in a steric clash of the *N7*-CH_3 and the *N1*-CH_3 groups in **9** restricts the conformation and positions the phenyl ring on top of the *N1*-CH_3 moiety (Fig. 11), resulting in the observed shielding effect, in the ^{1}H NMR, on the *N1*-CH_3 group in **9** as compared to that in **10**. This shielding effect of the phenyl group on the *N*1-CH_3 group (δ ≈ 1.1) was also observed for the *N7*-CH_3 analogs **11–17**. This provides an estimation of the solution conformation of the active analog **9** compared to the inactive analog **10**. In addition,

Table 5
Human cancer cell growth inhibitory activity GI_{50} (nM) of 9 in NCI 60 cell line panel.

Panel/Cell line	GI_{50} (nM)	Panel/Cell line	GI_{50} (nM)	Panel/Cell line	GI_{50} (nM)	Panel/Cell line	GI_{50} (nM)
Leukemia		**Colon Cancer**		**Melanoma**		**Renal Cancer**	
CCRF-CEM	9.96	COLO 205	9.78	LOX IMVI	8.53	786-0	13.23
HL-60 (TB)	11.23	HCC-2998	23.56	MALME-3M	12.07	A498	13.42
K-562	6.46	HCT-116	9.07	M14	10.56	ACHN	8.40
MOLT-4	19.85	HCT-15	5.14	MDA-MB-435	3.90	CAKI-1	15.72
RPMI-8226	15.29	HT29	7.60	SK-MEL-2	20.97	RXF 393	8.75
SR	9.64	KM12	10.76	SK-MEL-28	17.04	SN12C	15.76
NSCLC		SW-620	6.67	SK-MEL-5	14.58	TK-10	16.31
A549/ATCC	12.67	**CNS Cancer**		UACC-257	22.69	UO-31	10.01
EKVX	15.47	SF-268	12.17	UACC-62	15.90		
HOP-62	15.41	SF-295	11.43	**Ovarian cancer**		**Breast Cancer**	
HOP-92	16.03	SF-539	8.76	IGROVI	13.30	MCF7	10.81
NCI-H226	9.49	SNB-19	13.88	OVCAR-3	6.37	MDA-MB-231/ATCC	14.29
NCI-H23	11.87	SNB-75	10.81	OVCAR-4	12.93	HS 578T	11.19
NCI-H322M	14.09	U251	7.97	OVCAR-5	11.76	BT-549	24.12
NCI-H460	4.52	**Prostate Cancer**		OVCAR-8	14.69	T-47D	16.44
NCI-H522	14.43	PC-3	10.73	NCI/ADR-RES	8.24	MDA-MB-468	9.09
		DU-145	8.89	SK-OV-3	13.93		

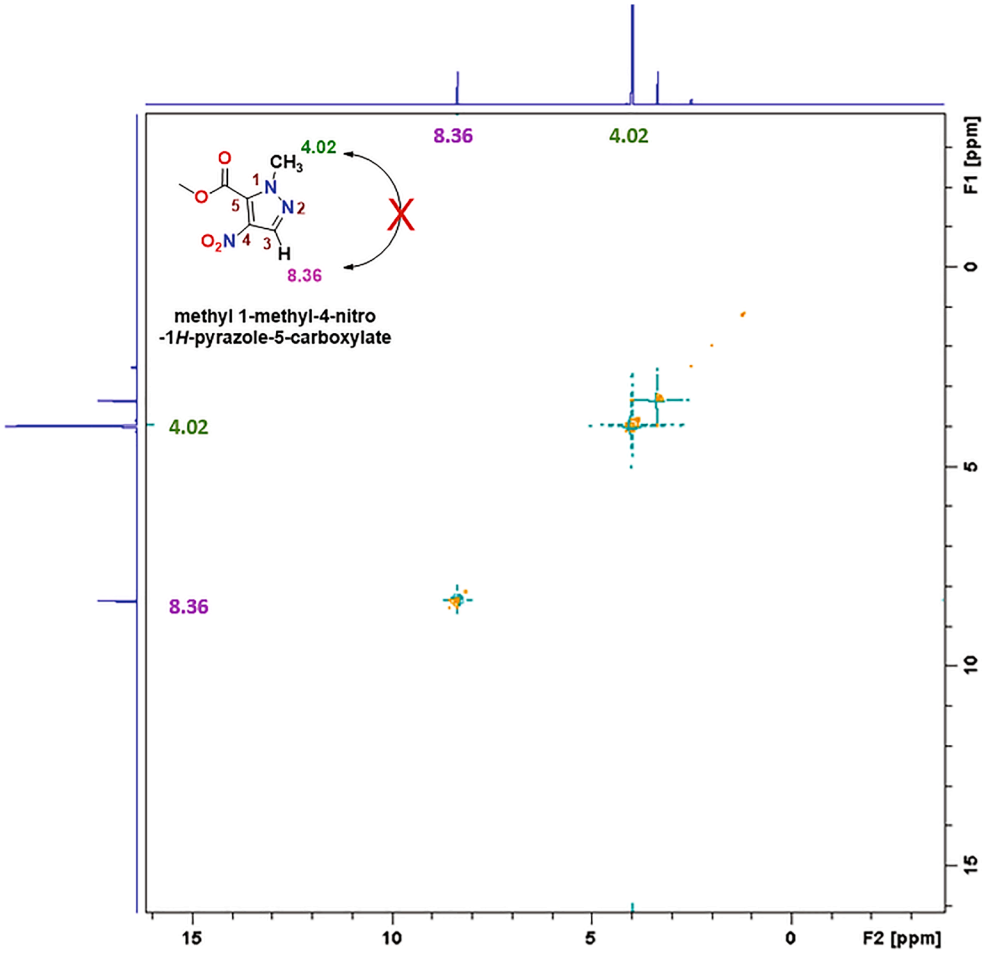

Fig. 7. NOESY NMR of Intermediate 29a.

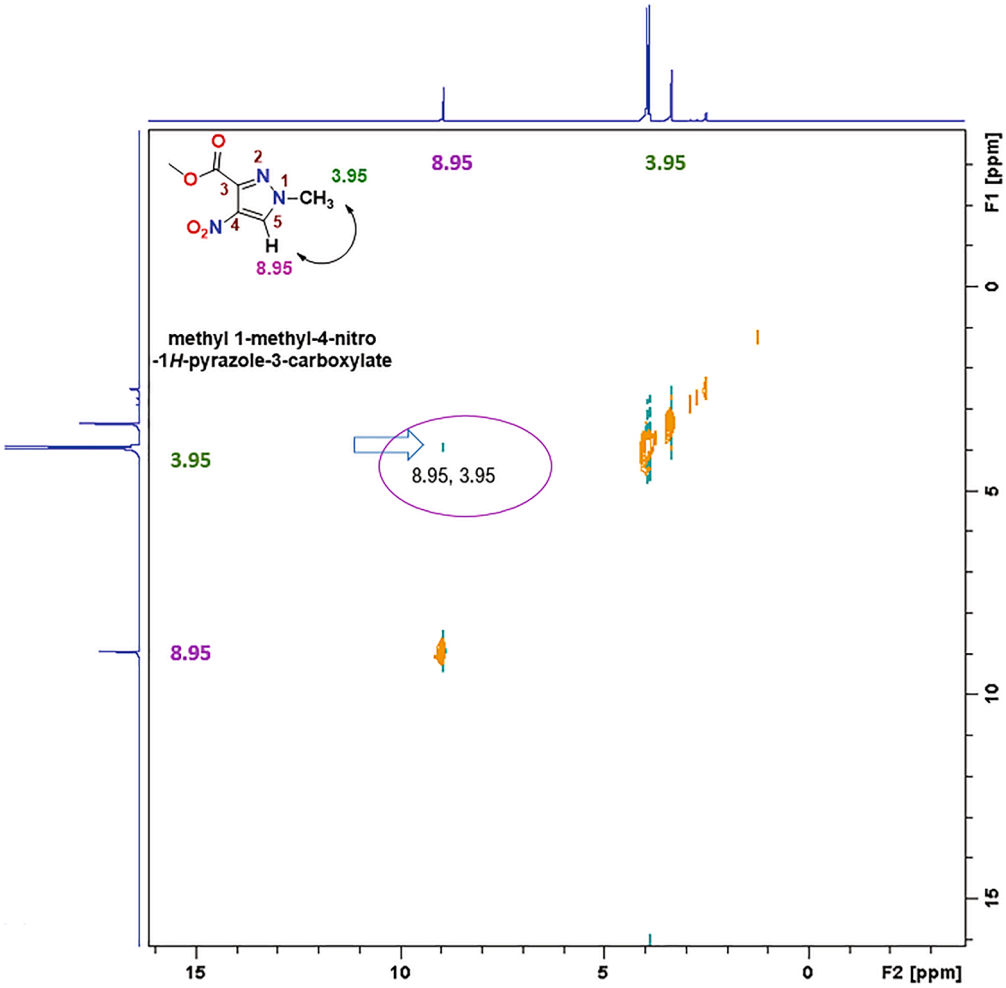

Fig. 8. NOESY NMR of Intermediate 29b.

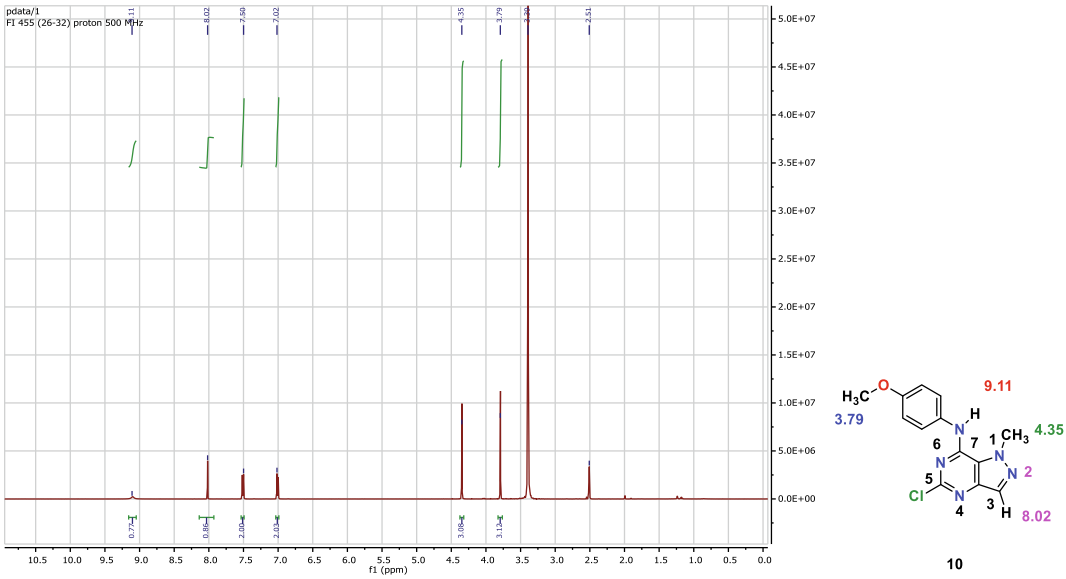

Fig. 9. ^{1}H NMR of 10.

the docked conformation of **9** in Fig. 5B is similar to the ^{1}H NMR solution conformation of **9**. This indicates a low energy barrier for **9** to adopt the bound conformation and results in potent activity.

In this study, a series of nine novel *N*1-methyl-pyrazolo[4,3-*d*]pyrimidines were designed and synthesized as anticancer agents that function as CS binding agents and as inhibitors of tubulin

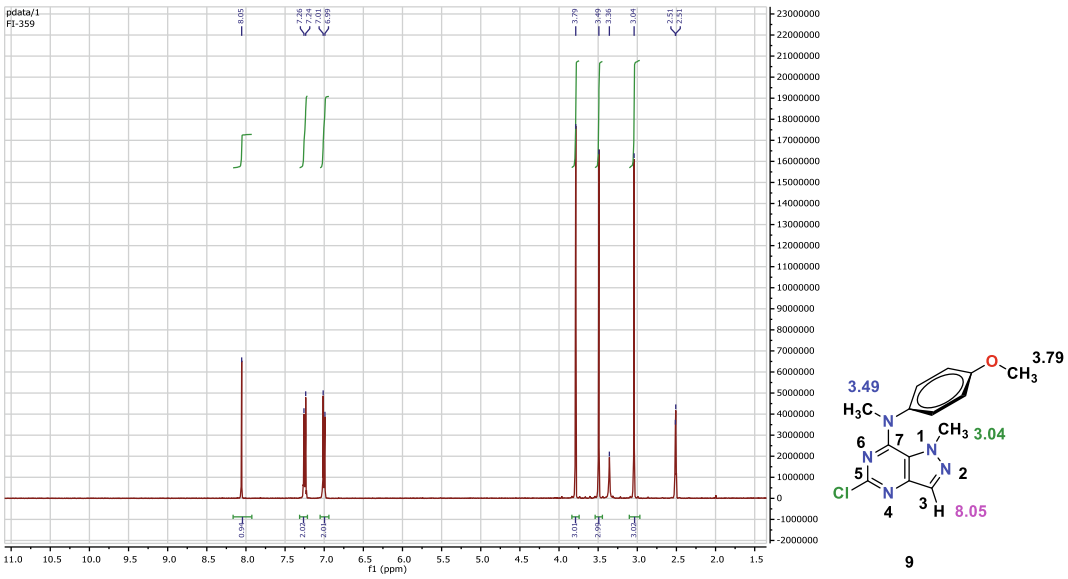

Fig. 10. ^{1}H NMR of 9.

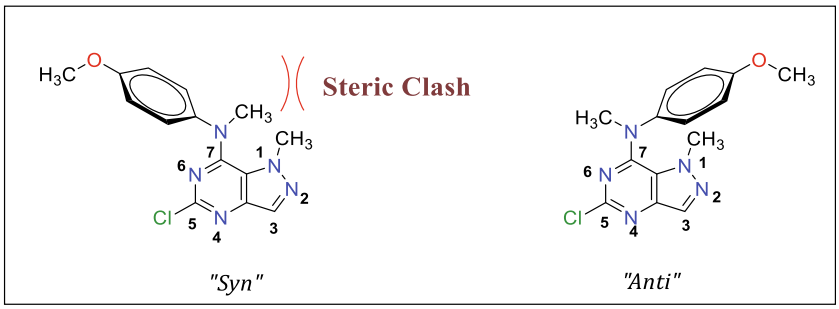

Fig. 11. Possible explanation of orientation of compound **9**.

polymerization. Synthesis of the target compounds involved alkylation of the pyrazolo scaffold to provide two regioisomers that were separated, characterized and structurally identified via ^{1}H NMR and NOESY spectroscopy. Compounds **9** and **11**–**13** strongly inhibited the polymerization of tubulin with IC_{50}s near ~0.5 μM., whereas compounds **14**–**16** inhibited the polymerization of tubulin with IC_{50s} near ~1 μM. Compounds **9**, **12**, **13** and **16** circumvented *β*III-tubulin mediated cancer cell resistance and compounds **9**–**17** circumvented Pgp mediated drug resistance. Compound **9** showed GI_{50} values ≤10 nM against many tumor cell lines, including several multidrug resistant phenotypes, in the standard NCI testing protocol. SAR studies indicated that the *N7*-CH_3 moiety of **9** was crucial for activity and that the 4′-$OMeC_6H_4$ was the best substitution for biological activity. In addition, the lower activity of **11** and **12** compared to **9** and **13** suggested that some flexibility of bond '*a*' and '*b*' were necessary for potent activity in this series. Compound **9** was significantly ($P < 0.0001$) better than paclitaxel at reducing MCF-7 TUBB3 (*β*III-tubulin overexpressing) tumor growth in an *in vivo* study and is poised for further preclinical development.

Declaration of Competing Interest

The authors declare that they have no known competing financial interests or personal relationships that could have appeared to influence the work reported in this paper.

Acknowledgements

We acknowledge the National Cancer Institute Developmental Therapeutics Program for performing the in vitro evaluation in the NCI 60-cell line panel. This work was supported, in part, by a grant from the National Institutes of Health, National Cancer Institute (CA142868 (to A.G), Duquesne University Adrian Van Kaam Chair in Scholarly Excellence (to A.G.); the CTRC Cancer Center Support Grant P30 CA054174 and the Flow Cytometry Shared Resource; and by an NSF equipment grant for NMR instrumentation (NMR: CHE 0614785). This research was supported in part by the Developmental Therapeutics Program in the Division of Cancer Treatment and Diagnosis of the National Cancer Institute, which includes federal funds under Contract No. HHSN261200800001E. The content of this publication does not necessarily reflect the views or policies of the Department of Health and Human Services, nor does mention of trade names, commercial products, or organizations imply endorsement by the U.S. Government.

Appendix A. Supplementary data

Supplementary data to this article can be found online at https://doi.org/10.1016/j.bmcl.2021.127923.

References

1 https://www.who.int/news-room/fact-sheets/detail/cancer.
2 Poruchynsky MS, Komlodi-Pasztor E, Trostel S, Wilkerson, et al. Microtubule-targeting agents augment the toxicity of DNA-damaging agents by disrupting intracellular trafficking of DNA repair proteins. *Proc Natl Acad Sci USA*. 2015;112:1571–1576.
3 Binarova P, Tuszynski J. Tubulin: structure, functions and roles in disease. *Cells*. 2019;8.

4 Coulup SK, Georg GI. Revisiting microtubule targeting agents: alpha-Tubulin and the pironetin binding site as unexplored targets for cancer therapeutics. *Bioorg Med Chem Lett*. 2019;29:1865–1873.
5 Field JJ, Kanakkanthara A, Miller JH. Microtubule-targeting agents are clinically successful due to both mitotic and interphase impairment of microtubule function. *Bioorg Med Chem*. 2014;22:5050–5059.
6 Steinmetz MO, Prota AE. Microtubule-targeting agents: strategies to hijack the cytoskeleton. *Trends Cell Biol*. 2018;28:776–792.
7 Yi X, Zhong B, Smith KM, Geldenhuys WJ, Feng Y, Pink JJ, et al. Identification of a class of novel tubulin inhibitors. *J Med Chem*. 2012;55:3425–3435.
8 Perez EA. Microtubule inhibitors: differentiating tubulin-inhibiting agents based on mechanisms of action, clinical activity, and resistance. *Mol Cancer Ther*. 2009;8: 2086–2095.
9 Du J, Li B, Fang Y, Liu Y, et al. Overexpression of Class III β-tubulin, Sox2, and nuclear Survivin is predictive of taxane resistance in patients with stage III ovarian epithelial cancer. *BMC Cancer*. 2015;15, 536-536.
10 Chiou JF, Liang JA, Hsu WH, Wang JJ, Ho ST, Kao A. Comparing the relationship of taxol-based chemotherapy response with P-glycoprotein and lung resistance-related protein expression in non-small cell lung cancer. *Lung*. 2003;181:267–273.
11 Binkhathlan Z, Lavasanifar A. P-glycoprotein inhibition as a therapeutic approach for overcoming multidrug resistance in cancer: current status and future perspectives. *Curr Cancer Drug Targets*. 2013;13:326–346.
12 Rosell R, Scagliotti G, Danenberg KD, et al. Transcripts in pretreatment biopsies from a three-arm randomized trial in metastatic non-small-cell lung cancer. *Oncogene*. 2003;22:3548–3553.
13 Seve P, Isaac S, Tredan O, Souquet P-J, Pacheco Y, Perol M, et al. Expression of class III β-tubulin is predictive of patient outcome in patients with non-small cell lung cancer receiving vinorelbine-based chemotherapy. *Clin Cancer Res*. 2005;11: 5481–5486.
14 Tommasi S, Mangia A, Lacalamita R, et al. Cytoskeleton and paclitaxel sensitivity in breast cancer: the role of β-tubulins. *Int J Cancer*. 2007;120:2078–2085.
15 Ferrandina G, Zannoni GF, Martinelli E, Paglia A, et al. Class III β-tubulin overexpression is a marker of poor clinical outcome in advanced ovarian cancer patients. *Clin Cancer Res*. 2006;12:2774–2779.
16 Hwang J-E, Hong J-Y, Kim K, et al. Class III β-tubulin is a predictive marker for taxane-based chemotherapy in recurrent and metastatic gastric cancer. *BMC Cancer*. 2013;13:8, 431/1-431/8.
17 Britten CD, Baker SD, Denis LJ, Johnson T, Drengler R, et al. Oral paclitaxel and concurrent cyclosporin A: targeting clinically relevant systemic exposure to paclitaxel. *Clin Cancer Res*. 2000;6:3459–3468.
18 Carlson K, Ocean AJ. Peripheral neuropathy with microtubule-targeting agents: occurrence and management approach. *Clin Br Cancer*. 2011;11:73–81.
19 Krens SD, McLeod HL, Hertz DL. Pharmacogenetics, enzyme probes and therapeutic drug monitoring as potential tools for individualizing taxane therapy. *Pharmacogenomics*. 2013;14:555–574.
20 Stengel C, Newman SP, Leese MP, Potter BV, Reed MJ, Purohit A. Class III beta-tubulin expression and in vitro resistance to microtubule targeting agents. *Br J Cancer*. 2010;102:316–324.
21 Arnst KE, Wang Y, Hwang DJ, et al. A potent, metabolically stable tubulin inhibitor targets the colchicine binding site and overcomes taxane resistance. *Cancer Res*. 2018;78:265–277.
22 Dong M, Liu F, Zhou H, Zhai S, Yan B. Novel natural product- and privileged scaffold-based tubulin inhibitors targeting thecolchicine binding site. *Molecules (Basel, Switzerland)*. 2016;21.
23 van Echteld I, Wechalekar MD, Schlesinger N, Buchbinder R, Aletaha D. Colchicine for acute gout. *Cochrane Database Syst Rev*. 2014;8, Cd006190.
24 McLoughlin EC, O'Boyle NM. Colchicine-binding site inhibitors from chemistry to clinic: A review. *Pharmaceuticals (Basel)*. 2020;13:8.
25 Ji YT, Liu YN, Liu ZP. Tubulin colchicine binding site inhibitors as vascular disrupting agents in clinical developments. *Curr Med Chem*. 2015;22:1348–1360.
26 Kaul R, Risinger AL, Mooberry SL. Microtubule-targeting drugs: more than antimitotics. *J Nat Prod*. 2019;82:680–685.
27 Pavana RK, Shah K, Gentile T, Dybdal-Hargreaves NF, et al. Sterically induced conformational restriction: Discovery and preclinical evaluation of novel pyrrolo [3,2-d]pyrimidines as microtubule targeting agents. *Bioorg Med Chem*. 2018;26: 5470–5478.
28 Pavana RK, Choudhary S, Bastian A, et al. Discovery and preclinical evaluation of 7-benzyl-N-(substituted)-pyrrolo[3,2-d]pyrimidin-4-amines as single agents with microtubule targeting effects along with triple-acting angiokinase inhibition as antitumor agents. *Bioorg Med Chem*. 2017;25:545–556.
29 Bajorath J. Computational scaffold hopping: cornerstone for the future of drug design? *Future Med Chem*. 2017;9:629–631.
30 Banerjee S, Arnst KE, Wang Y, et al. Heterocyclic-fused pyrimidines as novel tubulin polymerization inhibitors targeting the colchicine binding site: structural basis and antitumor efficacy. *J Med Chem*. 2018;61:1704–1718.
31 Maestro SR-S, LLC: New York, NY, 2019.
32 Devambatla RKV, Li W, Zaware N, et al. Design, synthesis, and structure-activity relationships of pyrimido[4,5-b]indole-4-amines as microtubule depolymerizing agents that are effective against multidrug resistant cells. *Bioorg Med Chem Lett*. 2017; 27:3423–3430.
33 Mallinson J, Collins I. Macrocycles in new drug discovery. *Future Med Chem*. 2012;4: 1409–1438.
34 Xiang W, Quadery TM, Hamel E, et al. The 3-D conformational shape of N-naphthyl-cyclopenta[d]pyrimidines affects their potency as microtubule targeting agents and their antitumor activity. *Bioorg Med Chem*. 2021;29, 115887.
35 Hao M-H. Theoretical calculation of hydrogen-bonding strength for drug molecules. *Chem Theory Comput*. 2006;2:863–872.
36 Golani LK, Islam F, O'Connor C, et al. Design, synthesis and biological evaluation of novel pyrrolo[2,3-d]pyrimidine as tumor-targeting agents with selectivity for tumor uptake by high affinity folate receptors over the reduced folate carrier. *Bioorg Med Chem*. 2020;28, 115544.
37 Squarcialupi L, Falsini M, Catarzi D, et al. Exploring the 2- and 5-positions of the pyrazolo[4,3-d]pyrimidin-7-amino scaffold to target human A1 and A2A adenosine receptors. *Bioorg Med Chem*. 2016;24:2794–2808.
38 Plummer MS, Cornicelli J, Roark H, et al. Discovery of potent, selective, bioavailable phosphodiesterase 2 (PDE2) inhibitors active in an osteoarthritis pain model, Part I: Transformation of selective pyrazolodiazepinone phosphodiesterase 4 (PDE4) inhibitors into selective PDE2 inhibitors. *Bioorg Med Chem Lett*. 2013;23:3438–3442.
39 Regiec A, Mastalarz H, Mastalarz A, Kochel A. Methylation of 4-nitro-3(5)-pyrazolecarboxylic acid. *Tetrahedron Lett*. 2009;50:2624–2627.
40 Grisham R, Ky B, Tewari KS, Chaplin DJ, Walker J. Clinical trial experience with CA4P anticancer therapy: focus on efficacy, cardiovascular adverse events, and hypertension management. *Gynecol Oncol Res Pract*. 2018;5, 1-1.
41 https://clinicaltrials.gov/ct2/show/NCT00113438.
42 Lin CM, Ho HH, Pettit GR, Hamel E. Antimitotic natural products combretastatin A-4 and combretastatin A-2: studies on the mechanism of their inhibition of the binding of colchicine to tubulin. *Biochemistry*. 1989;28:6984–6991.
43 Agarwal, N.; Nair, M. S.; Mazumder, A.; Poluri, K. M., Chapter 3 - Characterization of nanomaterials using nuclear magnetic resonance spectroscopy. In Characterization of Nanomaterials, Mohan Bhagyaraj, S.; Oluwafemi, O. S.; Kalarikkal, N.; Thomas, S., Eds. Woodhead Publishing: 2018; pp 61-102.